Silk fibroin microspheres as optical resonators for wide range humidity sensing and biodegradable lasers

SCHOLARONE™
Manuscripts

Silk fibroin microspheres as optical resonators for wide range humidity sensing and biodegradable lasers

Wey Yih Heah,[a] Hiroshi Yamagishi,[a] Keitaro Fujita,[a] Megumi Sumitani,[b] Yuya Mikami,[c] Hiroaki Yoshioka,[c] Yuji Oki,[c] Yohei Yamamoto,*[a]

Biopolymers, which are in definition organic macromolecules produced by living matter, are promising materials in terms of biodegradability and sustainability. However, in the field of optical sensing, most of the devices or their elements still rely on the synthetic inorganic or organic compounds. In this study, we successfully transform pristine silk fibroin (SF), a naturally abundant and eco-friendly material, into discrete, well-defined microspherical particles that function as an active optical resonator for precise moisture sensing over a wide humidity range. The SF self-assembles into microspherical particles upon water-in-oil emulsification. When being photoexcited, the SF microspheres, doped with fluorescent ionic dye, display whispering gallery mode (WGM) resonant luminescence. Because of the excellent hygroscopic property, the SF microspheres expand in size as increasing the surrounding humidity, and the WGM resonant peaks exhibit a red shift with a linear relation to the surrounding humidity over a wide humidity range up to 95 percent relative humidity (%RH) with the sensitivity as high as 187 pm/%RH. Furthermore, the SF microsphere works as a laser resonator upon femto-second pumping. The fully natural microspheres as presented in this work will serve as sustainable and environmentally friendly optical resonators and sensors.

Introduction

Unlike its analogues such as biodegradable and biocompatible ones, biopolymers are fully natural materials that can be readily decomposed in the ecological system. Besides, biopolymers are far more sustainable than the synthetic polymers that rely on the petroleum as the source. Although the processability or mechanical properties of biopolymers are generally incomparable to the well-established synthetic polymers, the refining technology has advanced so much[1–3]. Actually, some of the synthetic plastics in our lives, that is, plastic bags and straws, have already been replaced by the biopolymers or their derivatives with the aim to reduce the burden on the environment[4]. However, it still remains a fundamental challenge to develop biopolymer-based devices in the field of optics because of their poor optical performance and the immature micro-molding technology.

Optical humidity sensors, which is the focus of the present research, are one of the challenging targets since the

morphology, refractive index, and affinity toward moisture should be finely tuned to realize highly responsive and reliable sensors[5–9]. Namely, the polymers are expected to absorb a large volume of water vapour to make a subtle change in refractive index and optical path length, while the overall morphology and optical connection of the device should be kept intact. In fact, optical humidity sensors made of biopolymers (polypeptides, cellulose, etc.) reported so far suffer from a trade-off between the high-sensitivity and tolerance against the high-humidity environment[10–13].

Silk fibroin (SF) is a natural protein produced by Mulberry silkworm (*Bombyx mori*, Fig. 1a). SF is historically important merchandise, especially in the medieval times, as luxurious fabric[14,15]. Scientifically, SF is a semi-crystalline, highly oriented polypeptide fibre featuring rather high refractive index (~1.54), notable mechanical properties (toughness of 70–78 MJ m^{-3} and Young's modulus of 10–17 GPa), and moderate affinity toward moisture[16,17]. While pristine SF is insoluble to water or most organic solvents, SF is solution-processable by the use of aqueous solution of lithium bromide or Ajisawa reagent and is readily molded into diverse formats such as powder, fibre, film, tube and sponge[16,18–20]. These regenerated SFs maintain high biocompatibility and biodegradable properties and, thus, are applicable to tissue engineering, disease models, implantable devices, and drug delivery systems[18,21–24].

In the present study, we focus on the micrometre-scale molding of SF and successfully develop a SF-based optical microresonators with high sensitivity toward humidity even

a. Department of Materials Science and Tsukuba Research Center for Energy Materials Science (TREMS), Faculty of Pure and Applied Sciences, University of Tsukuba, 1-1-1 Tennodai, Tsukuba, Ibaraki 305-8573, Japan.
b. Division of Biotechnology, Institute of Agrobiological Sciences, National Agriculture and Food Research Organization (NARO), Owashi, Tsukuba, Ibaraki 305-8634, Japan.
c. Graduate School of Information Science and Electrical Engineering, Kyushu University, 744 Motooka, Nishi-ku, Fukuoka 819-0395, Japan.

Figure 1. (a) Photograph of silkworms (*Bombyx mori*). (b) Schematic representation of silk fibroin microsphere that expand or contract in response to the surrounding humidity. (c) Photograph of an aqueous dispersion of silk fibroin. (d) Electronic absorption (broken curve) and PL spectra (solid curve) of aqueous solution of AR52 (5.74 mM).
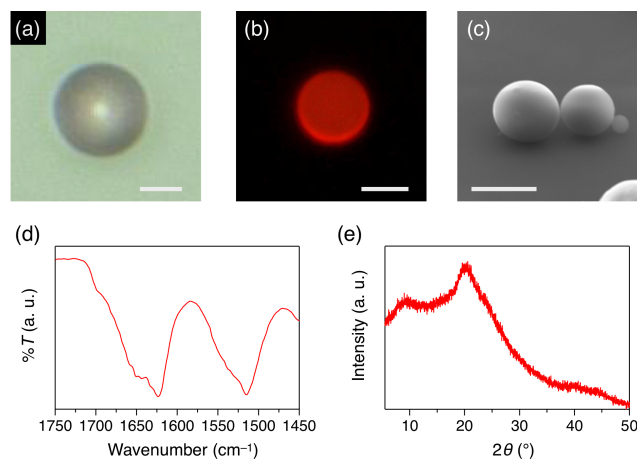

Figure 2. Optical microscopy (a), fluorescence microscopy (b) and SEM (c) images of the SF microspheres. Scale bars: 5 μm. FT-IR spectrum (d) and XRD pattern (e) of cast films of the SF microspheres.

under high-humidity environment (Fig. 1b). Natural SFs are processed into microspherical particles through degumming, dissolving and subsequent miniemulsification. The hardened microspheres are doped with ionic organic dye (AR52) to harness the photoluminescence (PL) property. The resultant microspheres exhibit whispering galley mode (WGM) optical resonance with excellent light confinement efficiency. The microspheres are mechanically and optically robust enough against strong pumping with a pulsed laser and thus work as a laser oscillator. The wavelengths of WGM resonance peaks are responsive against the change in the surrounding humidity with the sensitivity as high as 187 pm/%RH, which is kept intact even up to 95 %RH. The water absorption and desorption process can be repeated at least 6 times without losing the humidity sensing ability. Although some humidity sensors made of silk are reported which utilizes directly contacted taper fiber[11] and highly reflective Si substrate,[25] our humidity sensor utilizing SF microresonator is advantageous due to the non-contact (active resonator) and substrate-independent sensing.

Results and discussion

The SF microspheres were fabricated by modified mini-emulsion method using aqueous dispersion of SF (Fig. 1c) and Span80 as a non-ionic surfactant[26]. The resultant water-in-oil micelles containing SF were collected by centrifugation and washed with ethanol to remove the surfactant. For staining with a fluorescent dye, a portion of the SF powdery specimen (1 mg) was dispersed in a DMF solution of AR52 (1 mL, 300 μg mL^{-1}, Fig. 1d inset) and stood at 85 °C for 6 h. DMF swells the microspheres and allows for the dye diffuse into the SF matrix.

After cooling down to 25 °C, the dispersion was centrifuged twice to washout the residual dye to yield dye-doped SF microparticles with the doping level of the dye of 0.05 wt% (in details, see the Supplementary Information, Fig. S1).

The SF microparticle appears to be pale red (Fig. 2a) and emits orange-red photoluminescence (PL) homogeneously from the whole sphere (λ_{ex} = 460–495 nm, Fig. 2b). Further, PL spectra of the SF in a solution state and in a solid state (microsphere) are not so different (Fig. S2). These results indicate that the dyes are molecularly dispersed in the SF matrix. The detailed morphology of the resultant particles was visualized by means of scanning electron microscopy (SEM, Fig. 2c). The particles feature discrete spherical morphology and smooth surface. The average diameter of the resultant microspheres is 7.7 μm with a standard deviation of 3.0 μm (Fig. S3).

The spherical morphology and surface smoothness are attributed to the semi-crystallinity of the SF in the particles. Figure 2d shows Fourier-transform infrared spectra (FT-IR) of the SF microspheres in the amide I region (1600–1700 cm^{-1}), which is an authentic indicator of the secondary structure of peptide. The microspheres show a strong absorption band at 1623 cm^{-1} with a shoulder at 1644 cm^{-1}, which are attributed to the β-sheet and random coil structure, respectively[27]. Powder X-ray diffraction profile (XRD) of the microspheres exhibits broad diffraction band at 2θ = 20°, which is attributed to the stacking of the β-sheet (Fig. 2e)[28–30]. As reported in our previous paper, highly crystalline polymers are inappropriate for the formation of microspherical objects, since the smooth surface and round curvature typically requires certain softness of the materials[31]. We consider that partly amorphous aggregation of SF results in the well-defined microspheres with smooth surface morphology[32,33].
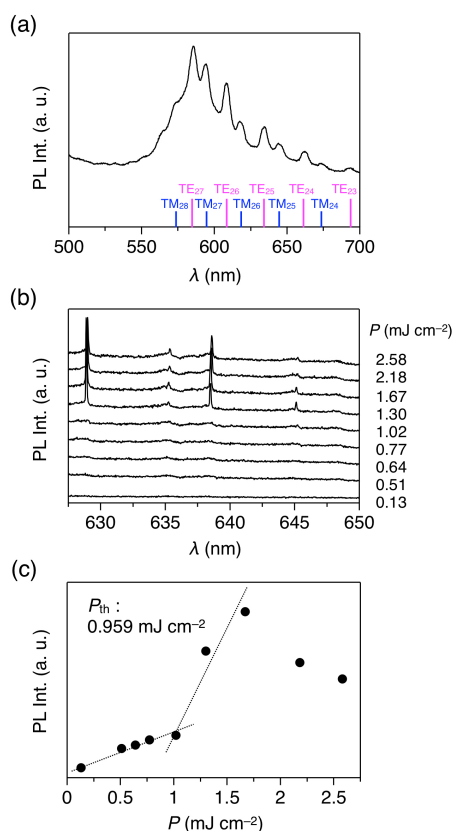
ARTICLE

Figure 3. (a) PL spectra of a single SF microsphere upon excitation with cw laser (λ_{ex} = 450 nm). Each WGM peak is assigned as shown on the bottom. (b) PL spectra of a single SF microsphere upon excitation with pulsed laser in various energy density (λ_{ex} = 565 nm, Δ = 100 fs, f = 1 kHz). (d) Plot of PL intensity of SF microsphere versus pumping energy density (P).

The microscopic photoluminescence (μ-PL) spectrum, obtained upon irradiation of a continuous-wave (cw) laser (λ_{ex} = 450 nm) to the rim of the individual SF microsphere, exhibits sharp and periodic resonant PL peaks, together with a broad spontaneous emission band from AR 52 (Fig. 3a). The resonant peaks are attributed the whispering gallery mode (WGM), generated by an interference of the confined PL inside the microsphere via total internal reflection at the polymer/air interface and are indexed as transverse electric (TE) and transverse magnetic (TM) modes[31,34]. Furthermore, the SF microsphere displays lasing upon femtosecond laser pumping (λ_{ex} = 565 nm, Δ = 100 fs, f = 1 kHz). When pumped with elevated power density (P), two sharp laser peaks emerge at 628 nm and 638 nm with a lasing threshold of 0.959 mJ cm^{-2} (Fig. 3b and c).

The humidity-dependent μ-PL spectroscopy was performed with a home-made gas-flowing chamber. The chamber is equipped with inlet and outlet gas tubes for flowing humidified air that are mixed with N$_2$ gas at a given ratio. The humidity in the chamber was continuously monitored with an electronics humidity sensor (Inkbird model IBS-TH1). The SF microspheres were spin-cast on a Si substrate, and the substrate was placed in the gas flowing chamber. A single SF microsphere (d = 3.9 μm) was irradiated with a focused cw laser (λ_{ex} = 450 nm, 50x

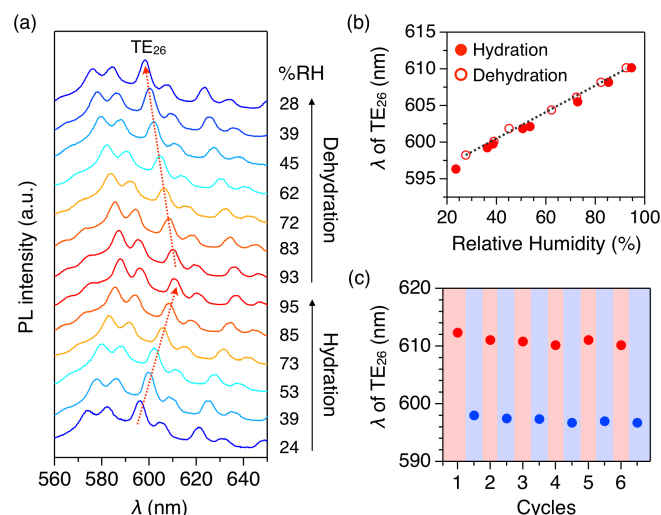**Figure 4.** (a) Humidity-dependent PL spectra of a single SF microsphere upon excitation with cw laser (λ_{ex} = 450 nm). (b) Plot of the wavelength of the resonant peak of TE$_{26}$ upon increasing (filled circle) and decreasing (open circle) the surrounding humidity. (c) Plot of the wavelength of the resonant peak of TE$_{26}$ upon 6 cycles of hydration (red) and dehydration (blue) between 93 and 25 %RH.

objective lens) through a glass ceiling, and the emission was guided to the spectrometer via an optical fiber. Each PL spectrum at a given humidity was measured after 5 min-incubation in the chamber.

The resonant peaks shift toward longer wavelength upon increasing the humidity and shift toward shorter wavelength upon decreasing the humidity (Fig. 4a). The peak shift is attributed to the absorption of moisture in the SF microsphere and subsequent increase in d of the microsphere. The plot of the peak wavelength of TE$_{26}$ mode against the relative humidity (Fig. 4b) exhibits a linear correlation with a responsivity of 187 pm/%RH. This value is almost constant for SF microspheres with different d (the average responsivity: 189 pm/%RH, Fig. S4). This is the first active resonator sensor made of natural polymer. Table S1 lists the responsivity and the applicable humidity range of humidity sensors made of different materials and techniques. The steepness and linearity of the responsivity is kept intact up to 95 %RH. Because the WGM peaks show red shift upon absorption of moisture, it is plausible that the contribution of the change of d is greater than that of the refractive index change: The absorption of moisture reduces the refractive index, which should lead to the blue shift of the WGM peaks. Assuming that the refractive index change is negligible, we can estimate that d of the SF microsphere change from 3.40 μm at 24 %RH to 3.49 μm at 95 %RH, using the theoretical equations (in details of the calculation, see SI).

The responsivity is maintained through repetition of hydration and dehydration cycles. Humidity is switched between 25 and 93 %RH with 5 min intervals for six times. Consequently, the resonant peak wavelength of TE$_{26}$ mode is switched upon hydration/dehydration cycles and keeps virtually

constant values for the hydrated and dehydrated conditions (Fig. 4c red and blue, respectively), demonstrating the chemical and physical robustness of SF microspheres. Our humidity sensor responses to the humidity change within 1 min, which is more rapid than the conventional humidity sensor we used as a reference (~5 min, Fig. S5). Note that the PL intensity decreases by half upon exposure to cw laser for 420 s, while the WGM peak shift is only 2 nm (Fig. S6). This result indicates that the peak shift by the humidity change is much larger (~14 nm by changing the humidity from 25 to 93 %RH), and the shrink by the laser excitation is not so much affected to the sensing performance.

Altogether, the SF microspheres overcome the conventional trade-off relationship between the water swelling ability and the mechanical robustness in high-humidity environment. Approximately, the co-existence of random coil and β-sheet structure is essential for realizing these properties. Random coil forms an amorphous structure with mechanical flexibility, while β-sheet forms mechanically rigid crystalline structure. As shown in Figure 2d and e, both random coil and β-sheet structures coexist in the semicrystalline SF microsphere, which provides mechanical flexibility and stiffness[16]. The moisture swelling in the random coil region enables the large volume change, while the β-sheet crystalline structure maintains the spherical morphology even after the swelling of large extent of water.

Conclusions

In this study, we successfully fabricate fluorescent AR52-doped silk fibroin (SF) microspheres that act as a WGM laser resonator and a robust humidity sensor. The SF microsphere features humidity sensitivity of 187 pm/%RH, which is the first active resonator sensor made of natural polymer. Furthermore, the SF resonator maintains its performance up to 95 %RH. The response is kept intact for at least six cycles of hydration and dehydration. The SF microspheres open up the application of biopolymers for safe, eco-friendly elements in the field of optics and lasers.

Author Contributions

H.Y., Y.Y. and M.S. designed the research, W.Y.H., K.F., Y.M., H.Y., and Y.O. performed the experiments, W.Y.H., H.Y. and Y.Y. prepared the manuscript.

Conflicts of interest

There are no conflicts to declare.

Acknowledgements

Notes and references

1   N. Jabeen, I. Majid, G. A. Nayik and F. Yildiz, Bioplastics and food packaging: A review, *Cogent Food Agric.*, 2015, **1**, 1117749.

2   A. Shafqat, A. Tahir, A. Mahmood, A. B. Tabinda, A. Yasar and A. Pugazhendhi, A review on environmental significance carbon foot prints of starch based bio-plastic: A substitute of conventional plastics, *Biocatal. Agric. Biotechnol.*, 2020, **27**, 101540.

3   F. Garavand, M. Rouhi, S. H. Razavi, I. Cacciotti and R. Mohammadi, Improving the integrity of natural biopolymer films used in food packaging by crosslinking approach: A review, *Int. J. Biol. Macromol.*, 2017, **104**, 687–707.

4   A. Soroudi and I. Jakubowicz, Recycling of bioplastics, their blends and biocomposites: A review, *Eur. Polym. J.*, 2013, **49**, 2839–2858.

5   Y. Peng, Y. Zhao, M. Q. Chen and F. Xia, Research Advances in Microfiber Humidity Sensors, *Small*, 2018, **14**, 1–20.

6   L. Labrador-Páez, K. Soler-Carracedo, M. Hernández-Rodríguez, I. R. Martín, T. Carmon and L. L. Martin, Liquid whispering-gallery-mode resonator as a humidity sensor, *Opt. Express*, 2017, **25**, 1165.

7   A. Chiasera, Y. Dumeige, P. Féron, M. Ferrari, Y. Jestin, G. N. Conti, S. Pelli, S. Soria and G. C. Righini, Spherical whispering-gallery-mode microresonators, *Laser Photonics Rev.*, 2010, **4**, 457–482.

8   J. Ward and O. Benson, WGM microresonators: Sensing, lasing and fundamental optics with microspheres, *Laser Photonics Rev.*, 2011, **5**, 553–570.

9   T. Reynolds, N. Riesen, A. Meldrum, X. Fan, J. M. M. Hall, T. M. Monro and A. François, Fluorescent and lasing whispering gallery mode microresonators for sensing applications, *Laser Photonics Rev.*, 2017, **11**, 1–20.

10   Y. Miao, K. Zhang, Y. Yuam, B. Liu, H. Zhang, Y. Liu and J. Yao, Agarose gel-coated LPG based on two sensing mechanisms for relative humidity measurement, *Appl. Opt.*, 2013, **52**, 90–95.

11   Z. Liu, W. Liu, C. Hu, Y. Zhang, X. Yang, J. Zhang, J. Yang and L. Yuan, Natural spider silk as a photonics component for humidity sensing, *Opt. Express*, 2019, **27**, 21946.

12   M. Eryürek, Z. Tasdemir, Y. Karadag, S. Anand, N. Kilinc, B. E. Alaca and A. Kiraz, Integrated humidity sensor based on SU-8 polymer microdisk microresonator, *Sensors Actuators, B Chem.*, 2017, **242**, 1115–1120.

13   A. Qiagedeer, H. Yamagishi, M. Sakamoto, H. Hasebe, F. Ishiwari, T. Fukushima and Y. Yamamoto, A highly sensitive humidity sensor based on an aggregation-induced emission luminogen-appended hygroscopic polymer microresonator, *Mater. Chem. Front.*, 2021, **5**, 799–803.

14   M. G. Uddin, Extraction of eco-friendly natural dyes from mango leaves and their application on silk fabric, *Text. Cloth. Sustain.*, 2015, **1**, 1–8.

15   T. B. Aigner, E. DeSimone and T. Scheibel, Biomedical Applications of Recombinant Silk-Based Materials, *Adv. Mater.*, 2018, **30**, 1–28.

16   L. D. Koh, Y. Cheng, C. P. Teng, Y. W. Khin, X. J. Loh, S. Y. Tee, M. Low, E. Ye, H. D. Yu, Y. W. Zhang and M. Y. Han, Structures, mechanical properties and applications of silk fibroin materials, *Prog. Polym. Sci.*, 2015, **46**, 86–110.

17   V. Fernández-Luna, J. P. Fernández-Blázquez, M. A. Monclús, F. J. Rojo, R. Daza, D. Sanchez-Dealcazar, A. L. Cortajarena and R. D. Costa, Biogenic fluorescent protein-silk fibroin phosphors for high performing light-emitting diodes, *Mater. Horizons*, 2020, **7**, 1790–1800.

18   D. N. Rockwood, R. C. Preda, T. Yücel, X. Wang, M. L. Lovett and D. L. Kaplan, Materials fabrication from Bombyx mori silk fibroin, *Nat. Protoc.*, 2011, **6**, 1612–1631.

19   E. S. Sashina, A. M. Bochek, N. P. Novoselov and D. A. Kirichenko, Structure and solubility of natural silk fibroin, *Russ. J. Appl. Chem.*, 2006, **79**, 869–876.

20   A. Ajisawa, Dissolution aqueous of silk fibroin with calciumchloride / ethanol solution, *J. Sericultural Sci. Japan*, 1997, **67**, 91–94.

21   M. Mondal and K. Trivedy, The silk proteins, sericin and fibroin in silkworm, Bombyx mori Linn., - a review, *Casp. J. Env. Sci*, 2007, **5**, 63–76.

22   H. Tao, D. L. Kaplan and F. G. Omenetto, Silk materials - A road to sustainable high technology, *Adv. Mater.*, 2012, **24**, 2824–2837.

23   E. Wenk, H. P. Merkle and L. Meinel, Silk fibroin as a vehicle for drug delivery applications, *J. Control. Release*, 2011, **150**, 128–141.

24   Z. Zhou, Z. Shi, X. Cai, S. Zhang, S. G. Corder, X. Li, Y. Zhang, G. Zhang, L. Chen, M. Liu, D. L. Kaplan, F. G. Omenetto, Y. Mao, Z. Tao and T. H. Tao, The Use of Functionalized Silk Fibroin Films as a Platform for Optical Diffraction-Based Sensing Applications, *Adv. Mater.*, 2017, **29**, 1–7.

25   Q. Li, N. Qi, Y. Peng, Y. Zhang, L. Shi, X. Zhang, Y. Lai, K. Wei, I. S. Kim and K. Q. Zhang, Sub-micron silk fibroin film with high humidity sensibility through color changing, *RSC Adv.*, 2017, **7**, 17889–17897.

26   S. J. Myung, H. S. Kim, Y. Kim, P. Chen and H. J. Jin, Fluorescent silk fibroin nanoparticles prepared using a reverse microemulsion, *Macromol. Res.*, 2008, **16**, 604–608.

27   C. Malinowski, F. He, Y. Zhao, I. Chang, D. W. Hatchett, S. Zhai and H. Zhao, Nanopatterned silk fibroin films with high transparency and high haze for optical applications, *RSC Adv.*, 2019, **9**, 40792–40799.

28   K. H. Lee, Silk sericin retards the crystallization of silk fibroin, *Macromol. Rapid Commun.*, 2004, **25**, 1792–1796.

29   D. Kuang, F. Wu, Z. Yin, T. Zhu, T. Xing, S. C. Kundu and S. Lu, Silk fibroin/polyvinyl pyrrolidone interpenetrating polymer network hydrogels, *Polymers (Basel).*, 2018, **10**, 16–18.

30   D. Kuang, F. Jiang, F. Wu, K. Kaur, S. Ghosh, S. C. Kundu and S. Lu, Highly elastomeric photocurable silk hydrogels, *Int. J. Biol. Macromol.*, 2019, **134**, 838–845.

31   S. Kushida, D. Braam, C. Pan, T. D. Dao, K. Tabata, K. Sugiyasu, M. Takeuchi, S. Ishii, T. Nagao, A. Lorke and Y. Yamamoto, Whispering Gallery Resonance from Self-Assembled Microspheres of Highly Fluorescent Isolated Conjugated Polymers, *Macromolecules*, 2015, **48**, 3928–3933.

32   J. Nam and Y. H. Park, Morphology of Regenerated Silk Fibroin: Effects of Freezing Temperature; Alcohol Addition, and Molecular Weight, *J. Appl. Polym. Sci.*, 2001, **81**, 3008–3021.

33   S. Kaewpirom and S. Boonsang, Influence of alcohol treatments on properties of silk-fibroin-based films for highly optically transparent coating applications, *RSC Adv.*, 2020, **10**, 15913–15923.

34   D. Okada, T. Nakamura, D. Braam, T. D. Dao, S. Ishii, T. Nagao, A. Lorke, T. Nabeshima and Y. Yamamoto, Color-Tunable Resonant Photoluminescence and Cavity-Mediated Multistep Energy Transfer Cascade, *ACS Nano*, 2016, **10**, 7058–7063.